CHEMISTRY
A EUROPEAN JOURNAL

DOI: 10.1002/chem.201002296

# Pure Trinuclear 4f Single-Molecule Magnets: Synthesis, Structures, Magnetism and Ab Initio Investigation

Fu-Sheng Guo,[a] Jun-Liang Liu,[a] Ji-Dong Leng,[a] Zhao-Sha Meng,[a] Zhuo-Jia Lin,[a] Ming-Liang Tong,*[a] Song Gao,*[b] Liviu Ungur,[c] and Liviu F. Chibotaru*[c]

**Abstract:** A family of linear $Dy_3$ and $Tb_3$ clusters have been facilely synthesized from the reactions of $DyCl_3$, the polydentate 3-methyloxysalicylaldoxime ($MeOsaloxH_2$) ligand with auxiliary monoanionic ligands, such as trichloroacetate, $NO_3^-$, $OH^-$, and $Cl^-$. Complexes **1**–**5** contain a nearly linear $Ln_3$ core, with similar Ln···Ln distances (3.6901(4)–3.7304(3) Å for the $Dy_3$ species, and 3.7273(3)–3.7485(5) Å for the $Tb_3$ species) and Ln···Ln···Ln angles of 157.036(8)–159.026(15)° for the $Dy_3$ species and 157.156(8)–160.926(15)° for the $Tb_3$ species. All three Ln centers are bridged by the two doubly-deprotonated $[MeOsalox]^{2-}$ ligands and two of the four $[MeOsaloxH]^-$ ligands through the $N,O$-$\eta^2$-oximato groups and the phenoxo oxygen atoms (Dy-O-Dy angles = 102.28(16)–106.85(13)°; Tb-O-Tb angles = 102.00(11)–106.62(11)°). The remaining two $[MeOsaloxH]^-$ ligands each chelate an outer $Ln^{III}$ center through their phenoxo oxygen and oxime nitrogen atoms. Magnetic studies reveal that both $Dy_3$ and $Tb_3$ clusters exhibit significant ferromagnetic interactions and that the $Dy_3$ species behave as single-molecule magnets, expanding upon the recent reports of the pure 4f type SMMs.

**Keywords:** ab initio investigation · cluster compounds · dysprosium · magnetic properties · single-molecule magnets

## Introduction

Since dodecanuclear manganese cluster was discovered as the first single-molecule magnet (SMM), numerous high-nuclearity homo- and heterometallic clusters have been obtained to date.[1,2] Due to the large inherent magnetic anisotropy of the lanthanide ions, heavy rare-earth metal systems, in particular dysprosium(III)-based complexes, have given rise to increasing interest in the area of molecular magnets.[3–6] Although interest toward mixed 3d/4d-4f SMM systems has rapidly developed in recent years,[3] pure lanthanide-based SMMs are extremely rare, owing to the difficulty in promoting magnetic interactions by the overlap of bridging ligand orbitals with the 4f orbitals of the lanthanide ions in these systems as a result of the efficient shielding of the unpaired electrons in the 4f orbitals.[7–9] So far, the reported pure 4f SMMs can be classified into three classes. The firstly confirmed class is the lanthanide single-ion SMMs of $Dy^{III}$, $Tb^{III}$, and $Ho^{III}$.[7] The second class is recently documented $Dy^{III}_3$ triangles,[8] which have an almost diamagnetic ground spin state, but show strong slow relaxation behavior within the excited states. The third class are ferromagnetically coupled polynuclear lanthanide(III) SMMs, with only a few examples; two recently reported 2D coordination polymers of dinuclear $Dy_2$ cores and one trinuclear $Dy_3$ cluster.[10] It is worth noting that ferromagnetically coupled polynuclear lanthanide(III) complexes are extremely rare,[11] not to mention the ferromagnetic polynuclear lanthanide(III) SMMs. In a sense, ligand design is thus one of the key aspects for achieving such interactions in pure lanthanide-based systems.

Recently, we focused on lanthanide coordination chemistry[6b] and speculated that the linear ligands with multichelating sites, for example, 3-methyloxysalicylald-oxime ($MeosaloxH_2$; Scheme 1),[6c] may be favorable for the formation of ferromagnetic pure lanthanide complexes through both potential single-atom $O_{phenolate}$ and two-atom $N{-}O_{oxime}$ bridges (Scheme 2).

---

[a] F.-S. Guo, J.-L. Liu, J.-D. Leng, Z.-S. Meng, Dr. Z.-J. Lin,
Prof. Dr. M.-L. Tong
Key Laboratory of Synthetic Bioinorganic Chemistry
of Ministry of Education
State Key Laboratory of Optoelectronic Materials and Technologies
School of Chemistry and Chemical Engineering
Sun Yat-Sen University, Guangzhou 510275 (P. R. China)
Fax: (+86) 20-8411-2245
E-mail: tongml@mail.sysu.edu.cn

[b] Prof. Dr. S. Gao
Beijing National Laboratory for Molecular Sciences
State Key Laboratory of Rare Earth Materials Chemistry
and Applications
College of Chemistry and Molecular Engineering
Peking University, Beijing 100871 (P. R. China)
Fax: (+86) 10-6275-1708
E-mail: gaosong@pku.edu.cn

[c] Dr. L. Ungur, Prof. Dr. L. F. Chibotaru
Division of Quantum and Physical Chemistry and
INPAC—Institute of Nanoscale Physics and Chemistry
Celestijnenlaan 200F, Katholieke Universiteit Leuven
3001 (Belgium)
Fax: (+32) 1632-7992
E-mail: Liviu.Chibotaru@chem.kuleuven.be

Supporting information for this article is available on the WWW under http://dx.doi.org/10.1002/chem.201002296.

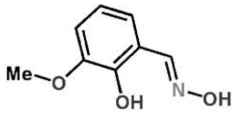

**MeosaloxH$_2$**

Scheme 1. The MeosaloxH$_2$ ligand with multichelating sites.

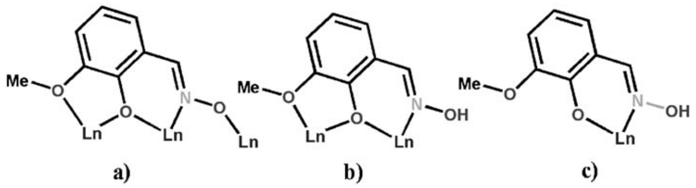

Scheme 2. Coordination modes of the [MeOsalox]$^{2-}$ and [MeOsaloxH]$^{-}$ ligands in complexes **1**–**5**.

We report herein a novel family of ferromagnetic linear trinuclear Dy$_3$ and Tb$_3$ complexes, [Dy$_3$(Meosalox)$_2$(MeosaloxH)$_4$(X)(Y)]·S (X/Y/S = OH/H$_2$O/MeOH·7H$_2$O for **1**; NO$_3$/MeOH/MeOH·0.5H$_2$O for **2**; Cl$_3$CCO$_2$/MeOH/MeOH for **3**), [Tb$_3$(MeOsalox)$_2$(MeosaloxH)$_4$(NO$_3$)(MeOH)]·MeOH·1.5H$_2$O (**4**), and [Tb$_3$(MeOsalox)$_2$(MeosaloxH)$_4$Cl(MeOH)][Tb$_3$(MeOsalox)$_2$(MeosaloxH)$_4$Cl(H$_2$O)]·H$_2$O (**5**), which provides a new facile synthetic route to the third-class of pure 4f SMMs. The MeOsaloxH$_2$ ligand adopts versatile coordination modes in complexes **1**–**5** (Scheme 2).

## Results and Discussion

**Description of the crystal structures**: *Linear trinuclear Dy$_3$ clusters of the MeOsaloxH$_2$ ligand (**1**–**3**)*: Structure **1** crystallizes in the space group $P2_1/c$, **2** and **3** crystallize in the space group $P\bar{1}$. Complexes **1**–**3** have similar linear trinuclear Dy$_3$ core structures (Figure 1), and the unique difference lies in that the mono-coordinated neutral ligand (Y) bound to Dy1 atom and the monoanion (X) bound to Dy3 atom. The X and Y are OH$^-$ and H$_2$O for **1**, NO$_3$$^-$ and MeOH for **2**, Cl$_3$CCO$_2$$^-$ and MeOH for **3**, respectively. All Dy atoms are eight-coordinate except the Dy3 atom in **2**,

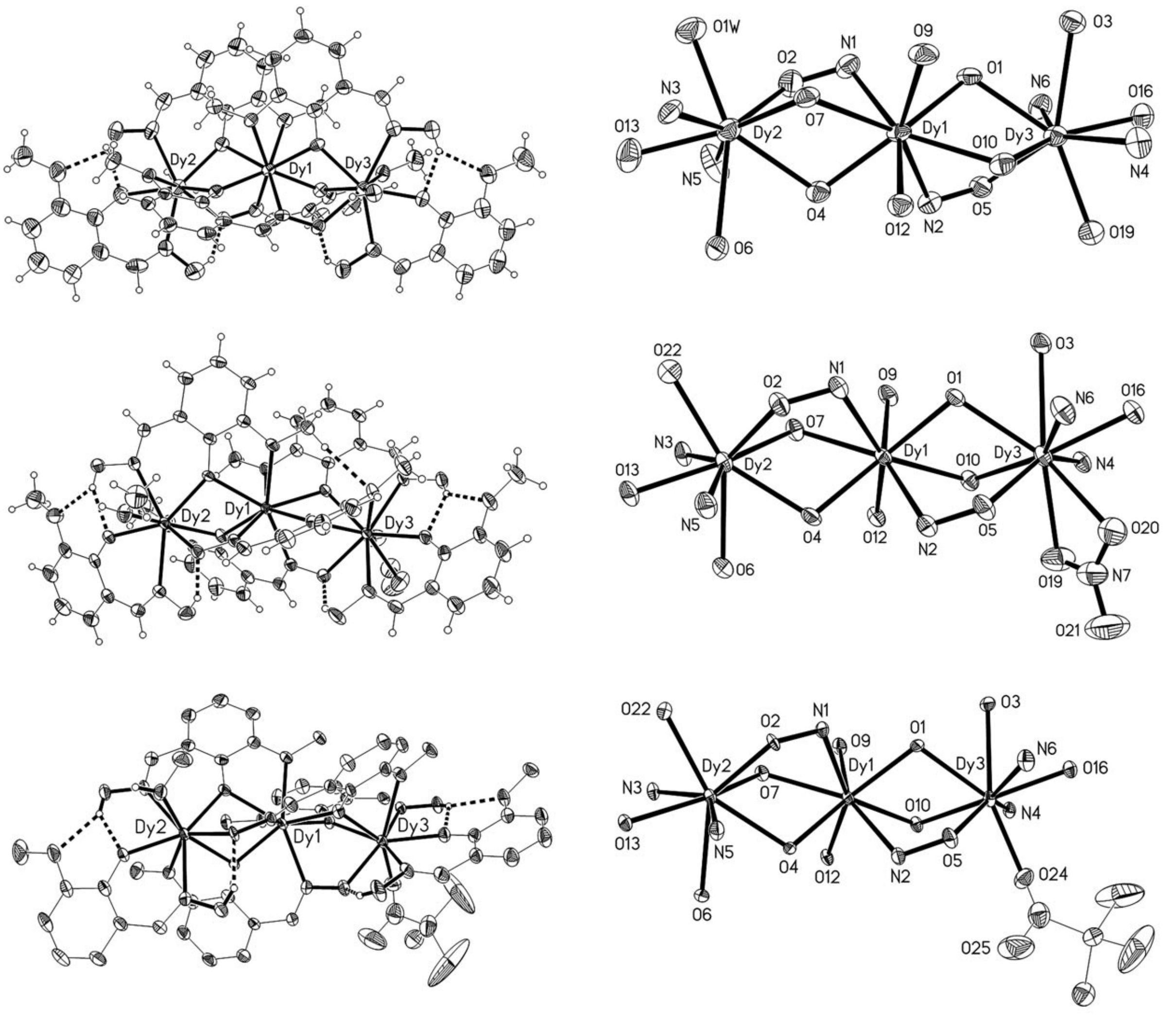

Figure 1. ORTEP drawings of molecular and core structures of **1** (top), **2** (middle), and **3** (bottom) with thermal ellipsoids at 50% probability.

which is in a nine-coordinate environment. Each of the terminal Dy1 atoms and the central Dy2 atom is surrounded by $O_6N_2$ atoms. The same donors bound to Dy3 atoms of **1**–**3** are five O atoms and two N atoms from one $[MeOsalox]^{2-}$ and three $[MeOsaloxH]^-$ ligands, and the different donors bound to Dy3 atoms of **1**–**3** are one terminal $OH^-$ (O19) for **1**, two O atoms from one chelated $NO_3^-$ anion for **2**, and one O atom from monodentate $Cl_3CCO_2^-$ for **3**. The three $Dy^{3+}$ ions are bridged by two couples of $\mu_3$:$\eta^2$:$\eta^1$:$\eta^1$-$[MeOsalox]^{2-}$ ligands through the single-atom $O_{phenolate}$ bridge with Dy-O-Dy angles of 102.36(12)–106.85(13)° and by a couple of two-atom $N{-}O_{oxime}$ bridges. Besides, a couple of $[MeOsaloxH]^-$ ligands act in $\mu$:$\eta^2$:$\eta^1$-chelating-bridging mode through the single-atom $O_{phenolate}$ bridges as well as the N donors. The remaining $[MeOsaloxH]^-$ groups only act as the chelating ligands. A lot of intramolecular $O_{oxime}{-}H{\cdots}O_{methyloxy/phenolate}$ hydrogen bonding interactions exist. The most striking structural feature is that the three structures have linear Dy3 cores with single-atom $O_{phenolate}$ bridges with Dy-O-Dy angles of 102.28(16)–106.46(16)° and two-atom $N{-}O_{oxime}$ bridges, quite different from that found for the other $Dy^{III}_3$ triangles.[8] The distances for Dy1···Dy2 and Dy2···Dy3 are 3.705 and 3.704 Å in **1**, 3.723 and 3.730 Å in **2**, and 3.709 and 3.690 Å in **3**, respectively, which can also be compared to those in the $Dy^{III}_3$ triangles[8] and to those found in recently documented dinuclear $Dy^{III}$ single-molecule magnets, and in a similar $Dy_3$ species.[10]

*Linear trinuclear $Tb_3$ clusters of the $MeOsaloxH_2$ ligand (**4** and **5**)*: The structures (Figure 2) of **4** and **5** are quite similar to that of **2** and **1**, respectively. Both **4** and **5** have similar linear trinuclear $Tb_3$ core structures though they crystallize in the space groups $P\bar{1}$ and $P2_1/n$, respectively. All Tb atoms are coordinated in an eight-coordinate environment except the Tb3 atom in **4**, which is nine-coordinate. Each of the terminal Tb2 (and Tb5 of **5**) atoms and the central Tb1 (and Tb4 of **5**) atom is surrounded by O6N2 atoms. The same donors bound to Tb3 (and Tb6 of **5**) atoms of **4** and **5** are five O atoms and two N atoms from one $MeOsalox^{2-}$ and three $MeOsaloxH^-$ ligands, and the different donors bound to Tb3 (and Tb6 of **5**) atoms of **4** and **5** are two O atoms from one chelated $NO_3^-$ anion for **4** and terminal $Cl^-$ for **5**. The three $Tb^{3+}$ ions are bridged by two couples of $\mu_3$:$\eta^2$:$\eta^1$:$\eta^1$-$MeOsalox^{2-}$ ligands through the single-atom $O_{phenolate}$ bridge with Tb-O-Tb angles of 102.00(11)–106.62(11)° and by a couple of two-atom $N{-}O_{oxime}$ bridges. Besides, a couple of $MeOsaloxH^-$ ligands act in $\mu_2$:$\eta^2$:$\eta^1$-chelating-bridging mode through the single-atom $O_{phenolate}$ bridges as well as the N donors. The remaining $MeOsaloxH^-$ groups only act as the chelating ligands. The unique differ-

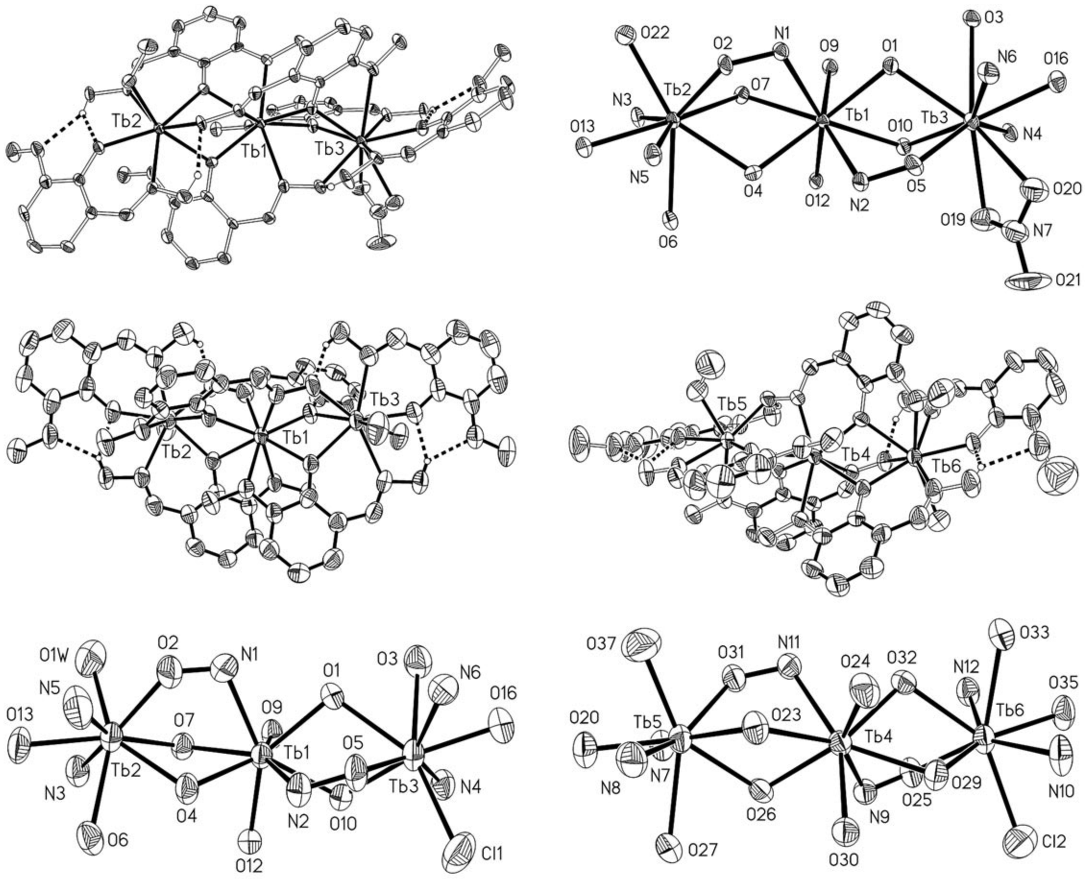

Figure 2. ORTEP drawings of molecular and core structures of **4** (top) and **5** (middle and bottom) with thermal ellipsoids at 50% probability.

ence lies in that the mono-coordinate neutral ligand (Y) bound to Tb2 atom and the monoanion (X) bound to Tb3 atom. The X and Y ligands are $NO_3^-$ and MeOH for **4**, $Cl^-$ and MeOH or $H_2O$ for **5**, respectively. An extended network of intramolecular $O_{oxime}$–H···$O_{methyloxy/phenolate}$ hydrogen bonding interactions exist.

**Magnetic properties of 1–3**: Direct current magnetic susceptibility studies were performed on polycrystalline sample of **1**–**3** in the 300–2 K range in an applied field (200 Oe for **1**, 400 Oe for **2** and **3**). The results are plotted as the $\chi_M T$ product versus $T$ in Figures 3a, 4a and 5a. At room temperature, the $\chi_M T$ values of 41.56, 41.06 and 42.87 $cm^3 K mol^{-1}$ for **1**–**3**, respectively, are in good agreement with the expected values of 42.50 $cm^3 mol^{-1} K$ for three free $Dy^{III}$ ions with the ground sate $^6H_{15/2}$ ($S = ^5/_2$, $L = 5$, $g = ^4/_3$).[3] As the temperature decreases to about 25 K, the $\chi_m T$ values decrease so little, that they almost remain unchanged. For complex **1**, the $\chi_M T$ reaches a minimum value of 40.24 $cm^3 K mol^{-1}$ at 26 K (38.55 $cm^3 K mol^{-1}$ at 20 K for **2**, and 41.41 $cm^3 K mol^{-1}$ at 23 K for **3**). Such unchanged susceptibility in the higher temperature range should therefore be ascribed to the balance between the effect of depopulation of the Stark components of $Dy^{3+}$; the intra-$Dy_3$ Dy···Dy ferromagnetic coupling through crystal-field effects are also expected to reduce the susceptibility. At lower temperature, the $\chi_M T$ curves increase dramatically, for compound **1**; the $\chi_M T$ reaches a value of 56.72 $cm^3 K mol^{-1}$ at 2.0 K (51.60 $cm^3 K mol^{-1}$ for **2**, and 57.36 $cm^3 K mol^{-1}$ for **3**), suggesting the presence of significant intra-$Dy_3$ Dy···Dy ferromagnetic interaction, which is less commonly observed in the polynuclear and polymeric dysprosium(III) complexes.[11,12]

The field-dependence of the magnetization of **1**–**3** show a fast increase in the magnetization at low magnetic fields (Figures 3a,4b, and Figure 5). For complex **1**, The $M$ versus $H$ plots below 10 K rises abruptly at low fields (inset of Figure 3a), which can be expected for ferromagnetically coupled compounds. At higher fields, M increases linearly and the maximum up to 7 T is 17.32 $\mu_B$, which is in relatively good agreement with the expected value (3×5.23 $\mu_B$) for three isolated $Dy^{III}$ ions. The lack of saturation on the $M$ versus $H$ data at 2.0 K suggests the presence of a significant anisotropy and/or low-lying excited states in these systems. For **2**, the $M$ value is 18.15 $\mu_B$ at 7 T, and16.03 $\mu_B$ for **3**. As the timescale of the quantum regime is relatively fast, the window of magnetic hysteresis loop at 0.5 K for **1** is not so evident (see Figure S1 in the Supporting Information).

AC magnetic susceptibility data for **1**–**3** do show frequency-dependent out-of-phase signals (Figures 3c/f, 4d/f, and 5d/f). The magnetization relaxation time ($\tau$) is derived from the frequency-dependence measurements and is plotted as a function of 1/$T$ in Figures 3g, 4g, and 5g. The profiles of these plots are unambiguous and characteristic of a single-molecule magnet for they show the onset of a slow relaxation regime of the magnetization on the measurement timescale. The best fitting the experimental data to the Arrhenius equation, $1/T_p = -k_B/\Delta[\ln(2\pi f) + \log\tau_0]$, gives $\tau_0 = 5.04 \times 10^{-7}$ s and $\Delta/k_B = 37.83$ K for **1**, $\tau_0 = 1.55 \times 10^{-6}$ s and $\Delta/k_B = 39.35$ K for **2**, and $\tau_0 = 1.07 \times 10^{-7}$ s and $\Delta/k_B = 39.79$ K for **3**. The similar slow relaxation behaviors observed in **1**–**3** are probably resulted from their structural similarity.[8,10]

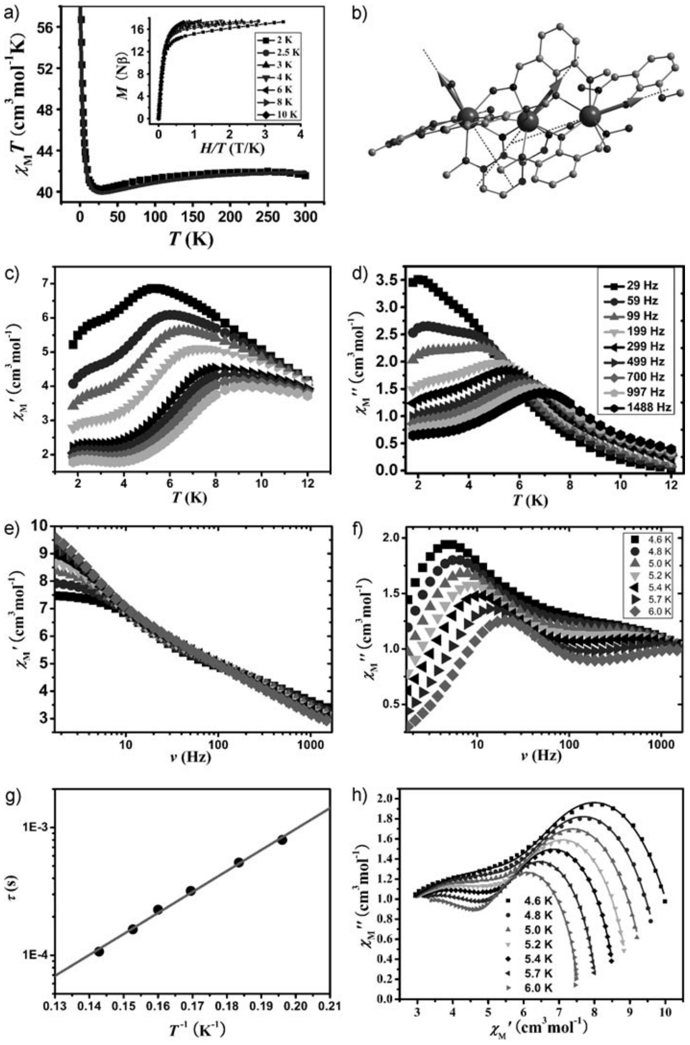

Figure 3. a) Temperature dependence of the $\chi_M T$ products at 400 Oe for **1**; the continuous line shows the simulated $\chi_M T$ for **1** (see the text). Inset: Plot of reduced magnetization ($M$/Nβ) versus $H/T$ in the temperature range 2-10 K. b) The arrangement of local anisotropy axes on Dy sites for **1**. Temperature dependence of c) the in-phase ($\chi'$) and d) the out-of-phase ($\chi''$b) ac susceptibility component at different ac frequency for **1** ($H_{ac} = 5$ Oe and $H_{dc} = 0$). Frequency dependence of e) the in-phase ($\chi'$) and f) out-of-phase ($\chi''$) ac susceptibility from 4.6 to 6.0 K under zero dc field. g) Magnetization relaxation time ($\tau$) versus $T^{-1}$ plot; the solid lines correspond to the Arrhenius law. h) Cole–Cole plot using the ac susceptibility data for **1**; the solid lines are the best fit obtained with a modified Debye function.

Cole–Cole diagrams of **1**–**3** ($\chi''$ versus $\chi'$ plot shown in Figure 3h, 4h and 5h) were obtained by using the Debye functions.[13] Complexes **2** and **3** illustrate probably the presence of only one relaxation process, as they exhibit a quasi-semicircle shape that can be fitted to the generalized Debye model with $\alpha < 0.28$ (**2**) and $\alpha < 0.20$ (**3**), while for com-

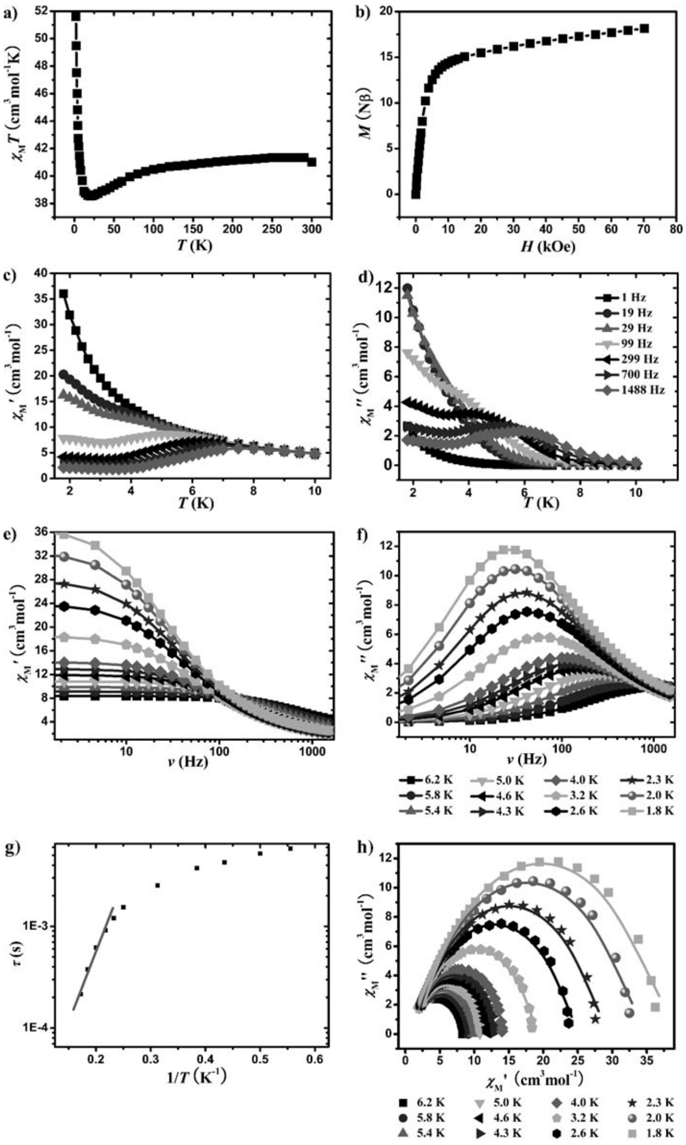

Figure 4. a) Temperature dependence of $\chi_M T$ plots of **2** at 400 Oe. b) Magnetization ($M$) vers field ($H$) at applied fields of 0–70 kOe at 2 K. Temperature dependence of c) the in-phase ($\chi'$) and d) the out-of-phase ($\chi''$) ac susceptibility component at different ac frequency ($H_{ac} = 5$ Oe and $H_{dc} = 0$). Frequency dependence of e) the in-phase and f) out-of-phase ac susceptibility from 1.8 to 6.2 K under zero dc field. g) Magnetization relaxation time ($\tau$) versus $T^{-1}$ plot; the solid lines correspond to the Arrhenius law. h) Cole–Cole plot using the ac susceptibility data for **2**; the solid lines are the best fit obtained with a generalized Debye model (with α always smaller than 0.28).

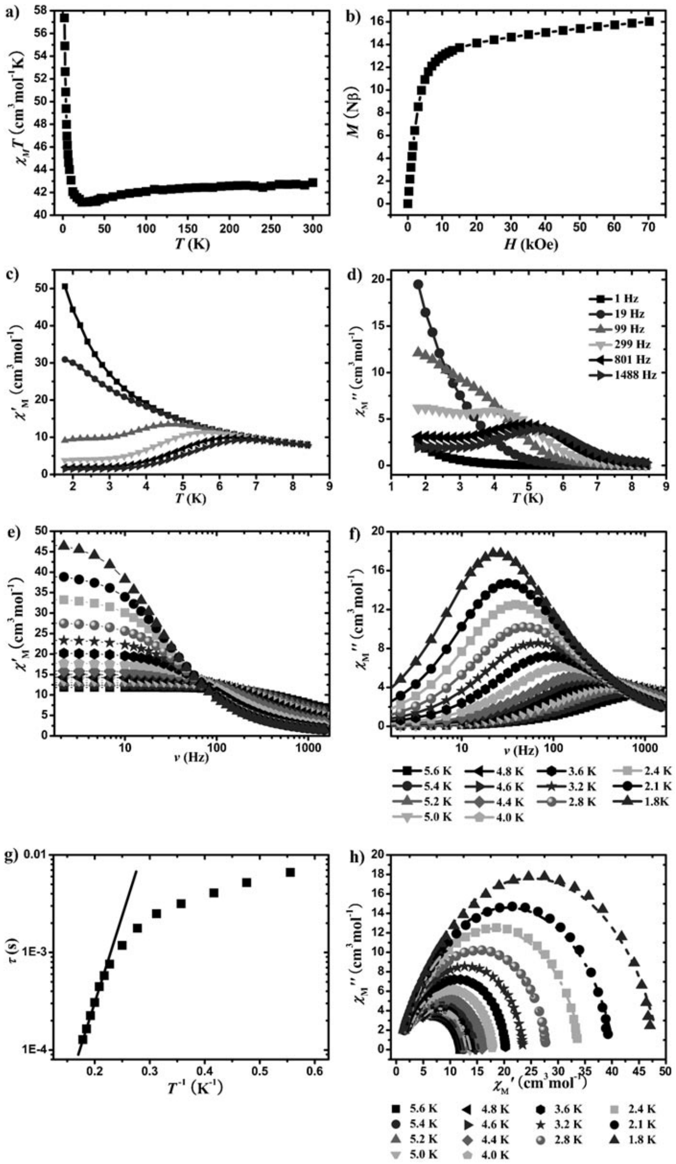

Figure 5. a) Temperature dependence of $\chi_M T$ plots of **3** at 400 Oe. b) Magnetization ($M$) vers field ($H$) at applied fields of 0–70 kOe at 2 K. Temperature dependence under zero-dc field of c) the in-phase ($\chi'$) and d) the out-of-phase ($\chi''$) ac susceptibility component at different ac frequency. Frequency dependence of e) the in-phase ($\chi'$) and f) the out-of-phase ($\chi''$) ac susceptibility from 1.8 to 5.6 K under zero dc field. g) Magnetization relaxation time ($\tau$) versus $T^{-1}$ plot; the solid lines correspond to the Arrhenius laws. h) Cole–Cole plot using the ac susceptibility data, the solid lines are the best fit obtained with a generalized Debye model (with α always smaller than 0.20).

pound **1**, two separate relaxation processes are clearly observed at higher temperature (5.7 and 6.0 K) that can be nicely described by the sum of two modified Debye functions.[13b–d] It is interesting to note that two maxima are observed in the frequency-dependent ac susceptibility. These findings, along with Cole–Cole plots showing quasi-semicircles and fitting Debye functions for compound **1** (see Figure 3h and Table S1 in the Supporting Information) indicate the presence of multiple slow relaxation processes.

**Magnetic properties of 4 and 5**: At room temperature, the $\chi_M T$ values are 34.69 and 34.31 cm$^3$ Kmol$^{-1}$ for **4** and **5** (Figure 6a and 7b), respectively, which are close to those (35.46 cm$^3$ mol$^{-1}$ K) expected for three free Tb$^{III}$ ions with the ground sate $^7F_6$ and $g = {}^3/_2$,[3b] respectively. On lowering the temperature, the $\chi_M T$ product gradually decreases before reaching a minimum value of 31.6 cm$^3$ Kmol$^{-1}$ at 20 K. The value of $\chi_M T$ then increases sharply to a maximum value of 40.49 cm$^3$ Kmol$^{-1}$ (**4**) and 40.23 cm$^3$ Kmol$^{-1}$

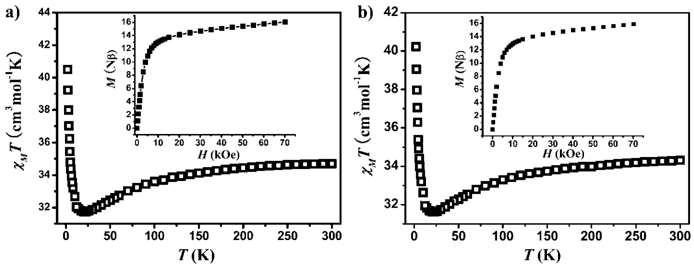

Figure 6. a) Plot of $\chi T$ versus $T$ for **4** at 200 Oe. Inset: Magnetization ($M$) vers field ($H$) at applied fields of 0–70 kOe at 2 K. b) Temperature dependence of the $\chi T$ products at 400 Oe for **5**. Inset: $M$ versus $H$ at applied fields of 0–70 kOe at 2 K.

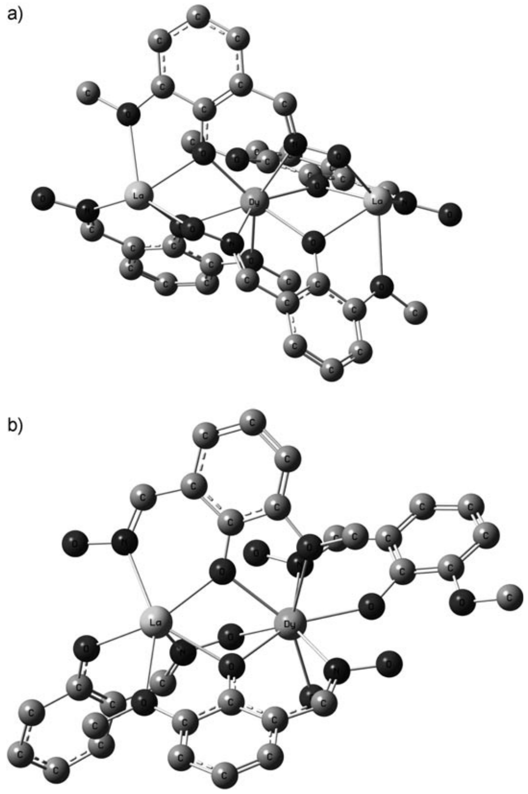

Figure 7. Structure of the calculated fragments of the complex **1**: the central $Dy^{3+}$ ion (fragment Dy1) a) and the marginal $Dy^{3+}$ ion (fragment Dy2) b). The other marginal $Dy^{3+}$ fragment (fragment Dy3) has similar structure to the fragment Dy2, with slightly different bond lengths and angles.

(**5**) at 2.0 K, revealing the presence of intra-$Tb_3$ Tb···Tb ferromagnetic interactions, which is only rarely observed in polynuclear pure $Tb^{III}$ complexes.[3]

The field dependence of magnetization at 2 K shows a sharp increase at low magnetic fields (insets in Figure 6a and 6b), indicating the fast magnetization, which shows that ferromagnetic interactions take place within the spin carriers. the magnetization increases slowly reaching at 7 T the value of 16.03 $\mu_B$ (**4**) and 15.89 $\mu_B$ (**5**) without clear saturation as a result of the presence of anisotropy, but the dynamic susceptibilities suggest that there are no frequency-dependent out-of-phase signals, so **4** and **5** are not SMMs.

**Ab initio calculations and simulation of magnetism in 1**: Complexes of **1**–**3** have similar core structures, therefore, only ab initio calculations and simulation of magnetism in **1** are discussed here in detail. To have an insight into the magnetic properties of the complex **1**, we performed fragment ab initio calculations of each magnetic center of the complex. In these calculations, the effects of the neighboring dysprosium atoms were simulated by closed-shell $La^{3+}$-embedding ab initio model potential (AIMP).[14] The fragment models for central (Dy1) and marginal (Dy2 and Dy3) $Dy^{3+}$ ions included all ligands which make bonds with the corresponding $Dy^{3+}$ ion of that fragment, while the ligands which have bonds exclusively to the neighbouring $Dy^{3+}$ ions were removed. The structure of the calculated fragments is shown in Figure 7.

All calculations on model fragments were performed with MOLCAS 7.4 program package.[15] The relativistic effects were treated in two steps, both based on Douglas–Kroll–Hess Hamiltonian.[16] In the first step, we used appropriate basis sets which included scalar relativistic terms for the determination of the spin-free wave functions and energies in the complete active space self-consistent field (CASSCF) calculations. In the second step, the spin-orbit coupling was included by restricted active space state interaction (RASSI) method, with the CASSCF solutions taken as input states. Next, the resulting spin-orbit eigenstates were used as input for the SINGLE ANISO program,[17] which computed all magnetic properties of the fragments.

All the atoms were represented by basis sets of atomic natural orbitals from the ANO-RCC basis library, as implemented in MOLCAS 7.4 package. The following contractions were used for the $Dy^{3+}$ and the atoms from the first coordination sphere: [8s7p5d4f2g1h] for Dy; [4s3p2d] for O and N. The distant atoms were represented by slightly smaller basis sets: [3s2p] for C, N and O; [2s] for H. The active space consisted of nine electrons spanning the Dy 4f seven orbitals [CAS(9,7)]. This is a reasonable dimension of the active space, since the 4f orbitals usually show a very weak hybridization with the ligands' orbitals. The CASSCF state average calculations of all sextets, quartets, and doublets were performed. The spin-orbit interaction was computed within all sextets, 128 quartets and 130 doublets states within the RASSI program.

The energies of the lowest Kramers doublets of each fragment are shown in Table 1. Table 2 shows the main values of the gyromagnetic tensor of the lowest Kramers doublet of three dysprosium fragments. The arrangement of local anisotropy axes are shown in Figure 3b. Although these axes are far from being parallel to each other, they lie practically in one plane.

The ground Kramers doublet on each dysprosium ion is separated from the first excited one by a gap $> 50\,cm^{-1}$ (Table 1), which is a priori larger than any exchange interaction between them. Therefore for the description of low-

Table 1. Energies of the lowest Kramers doublets of **1** [$cm^{-1}$].

| | Dy1 | Dy2 | Dy3 |
|---|---|---|---|
| 1 | 0.000 | 0.000 | 0.000 |
| 2 | 54.284 | 100.662 | 233.724 |
| 3 | 133.599 | 205.016 | 278.933 |
| 4 | 175.540 | 300.544 | 300.771 |
| 5 | 237.550 | 392.078 | 350.885 |
| 6 | 327.825 | 459.846 | 406.778 |
| 7 | 362.735 | 600.213 | 464.476 |
| 8 | 378.683 | 647.975 | 607.263 |
| 9 | 3579.669 | 3589.818 | 3660.477 |

Table 2. Main values of the **g** tensors of the lowest Kramers doublets on Dy sites of **1**.

| | Dy1 | Dy2 | Dy3 |
|---|---|---|---|
| $g_X$ | 0.049 | 0.056 | 0.003 |
| $g_Y$ | 0.149 | 0.107 | 0.005 |
| $g_Z$ | 18.990 | 19.630 | 19.760 |
| angle with the main magnetic axis on Dy1 | | | |
| | 0.0 | 25.85 | 21.92 |

lying exchange multiplets of the whole complex **1** we consider that only the ground Kramers doublet of each $Dy^{3+}$ is involved in the exchange interaction. The high value of $g_Z$ on the dysprosium ions (Table 2) points on an essentially axial nature of the ground Kramers doublet,[18a] therefore, the exchange interaction among the $Dy^{3+}$ centers will be close to Ising type [Eq. (1)].[18b,c]

$$\hat{H} = -J\left(\tilde{S}_Z^{\mathrm{Dy1}}\,\tilde{S}_Z^{\mathrm{Dy2}} + \tilde{S}_Z^{\mathrm{Dy1}}\,\tilde{S}_Z^{\mathrm{Dy3}}\right) \tag{1}$$

In Equation (1) $\tilde{S}_Z^{\mathrm{Dy}i}$ is the projection of the pseudospin $\tilde{S} = 1/2$ on the anisotropy axis of the corresponding $Dy_i$ ion (Figure 3 d). The simulations of magnetic properties of the complex have been done with the program POLY ANISO, which uses as input the data from ab initio fragment and SINGLE ANISO calculations. The calculated powder susceptibility for $J = 7.5\ cm^{-1}$ (the only fitting parameter) is shown in Figure 3 a.

**Ab initio calculations and simulation of magnetism in 4**: Similar fragment ab initio calculations were performed for complex **4**. Isostructural fragments with those shown in Figure 7 were considered for the central and two lateral terbium ions. The lowest energy levels on $Tb^{3+}$ sites are shown in Table 3.

It is quite surprising that the crystal-field splitting of the lowest $^7F_6$ multiplet of the $Tb^{3+}$ ion leaves the lowest two levels almost degenerate. These two lowest levels forming a non-Kramers doublet can be considered components of an effective spin $\tilde{S} = 1/2$. The main values of the **g** tensor calculated in the basis of the two lowest states reveals a pure Ising-type local magnetizations on $Tb^{3+}$ sites (Table 4).

Therefore the Ising model for the exchange interactions, described by Equation (1), is also applicable in this case.

Table 3. Energies of the lowest levels of **4** [$cm^{-1}$].

| | Tb1 | Tb2 | Tb3 |
|---|---|---|---|
| 1 | 0.000 | 0.000 | 0.000 |
| 2 | 0.131 | 0.029 | 0.090 |
| 3 | 22.579 | 142.214 | 106.225 |
| 4 | 26.390 | 144.587 | 107.496 |
| 5 | 59.529 | 235.247 | 171.446 |
| 6 | 80.723 | 242.520 | 178.386 |
| 7 | 100.832 | 292.435 | 214.780 |
| 8 | 148.959 | 330.380 | 235.191 |
| 9 | 154.370 | 356.951 | 242.988 |
| 10 | 275.726 | 390.849 | 275.819 |
| 11 | 279.138 | 402.843 | 277.512 |
| 12 | 347.074 | 623.244 | 485.772 |
| 13 | 348.359 | 623.458 | 485.818 |
| 14 | 2095.135 | 2227.202 | 2153.189 |

Table 4. Main values of the **g** tensors of the lowest effective $\tilde{S} = 1/2$ on Tb sites of **4**.

| | Tb1 | Tb2 | Tb3 |
|---|---|---|---|
| $g_X$ | 0.000 | 0.000 | 0.000 |
| $g_Y$ | 0.000 | 0.000 | 0.000 |
| $g_Z$ | 16.834 | 17.839 | 17.837 |

The directions of local main magnetic axes on Tb sites are shown in Figure 8 b. Their relative arrangement shows a stronger non-collinearity (ca 45° for the neighbouring sites) than in **1**. The calculated powder susceptibility for the exchange parameter $J = 2.9\ cm^{-1}$ (on the basis of the $\tilde{S} = 1/2$) is shown in Figure 8 a.

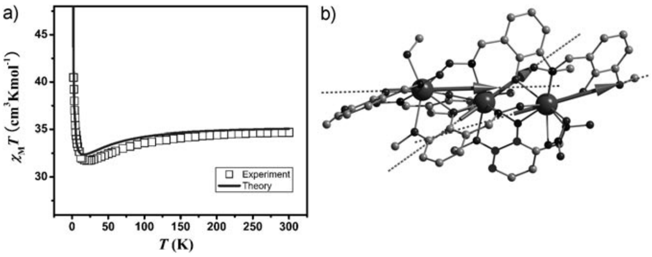

Figure 8. a) Temperature dependence of the $\chi T$ products at 200 Oe for **4**; the continuous line shows the simulated $\chi T$ for **4** (see the text). b) The arrangement of local anisotropy axes on Tb sites for **4**.

## Conclusion

In this study, we provide a facile synthetic route to rare ferromagnetic polynuclear lanthanide complexes towards pure 4f SMMs, including three new linear $Dy_3$ clusters exhibiting SMM behaviors, and two similar $Tb_3$ cluster analogues, isolated from the $LnCl_3$/3-methyloxysalicylaldoxime reaction system with different auxiliary ligands. Systematic ab initio investigation is carried out to explain the magnetism of both $Dy_3$ SMMs and ferromagnetic $Tb_3$ clusters. This work opens a promising route toward the design of new 4f magnetic materials.

Table 5. Crystal data and structure refinement for **1**–**5**.

| | **1** (150 K) | **2** (293 K) | **3** (150 K) | **4** (150 K) | **5** (293 K) |
|---|---|---|---|---|---|
| formula | $C_{49}H_{67}Dy_3N_6O_{28}$ | $C_{50}H_{55}Dy_3N_7O_{23.5}$ | $C_{52}H_{54}Cl_3Dy_3N_6O_{22}$ | $C_{50}H_{57}N_7O_{24.5}Tb_3$ | $C_{97}H_{100}Cl_2N_{12}O_{39}Tb_6$ |
| $M_r$ | 1675.59 | 1617.51 | 1708.86 | 1624.79 | 3082.31 |
| crystal system | monoclinic | triclinic | triclinic | triclinic | monoclinic |
| space group | $P2_1/c$ | $P\bar{1}$ | $P\bar{1}$ | $P\bar{1}$ | $P2_1/n$ |
| $a$ [Å] | 18.3328(7) | 10.7316(4) | 10.8481(4) | 10.6944(3) | 17.4982(5) |
| $b$ [Å] | 20.1606(6) | 15.1175(4) | 15.1498(7) | 14.9128(4) | 19.4175(3) |
| $c$ [Å] | 20.1214(7) | 18.8565(8) | 18.6580(8) | 18.7671(5) | 35.5740(7) |
| $\alpha$ [°] | 90 | 98.124(1) | 98.795(1) | 98.544(2) | 90 |
| $\beta$ [°] | 114.290(4) | 101.439(1) | 101.869(1) | 101.837(2) | 92.388(1) |
| $\gamma$ [°] | 90 | 94.420(1) | 96.794(1) | 93.858(2) | 90 |
| $V$ [Å$^3$] | 6778.5(4) | 2950.86(18) | 2929.8(2) | 2882.07(14) | 12076.5(5) |
| $Z$ | 4 | 2 | 2 | 2 | 4 |
| $\rho_{calcd}$ [g cm$^{-3}$] | 1.642 | 1.820 | 1.937 | 1.872 | 1.695 |
| $\mu$ [mm$^{-1}$] | 3.354 | 3.844 | 4.007 | 3.730 | 3.592 |
| $R_1$ [$I>2\sigma(I)$][a] | 0.0568 | 0.0396 | 0.0456 | 0.0358 | 0.0571 |
| $wR_2$ (all data)[b] | 0.1511 | 0.1029 | 0.1176 | 0.0702 | 0.1559 |

[a] $R_1 = \Sigma||F_o|-|F_c||/\Sigma|F_o|$, [b] $wR_2 = [\Sigma w(F_o^2-F_c^2)^2/\Sigma w(F_o^2)^2]^{1/2}$.

## Experimental Section

**Materials and physical measurements**: All of the starting materials employed were commercially available and used as received without further purification. The C, H, and N microanalyses were carried out with an Elementar Vario-EL CHNS elemental analyzer. The FT-IR spectra were recorded from KBr pellets in the range of 4000–400 cm$^{-1}$ on a Bio-Rad FTS-7 spectrometer.

**Synthesis of [Dy$_3$(MeOsalox)$_2$(MeosaloxH)$_4$(OH)(H$_2$O)]·MeOH·7H$_2$O (1)**: A mixture of *o*-vanillin (0.061 g, 0.4 mmol), hydroxylamine chloride (0.028 g, 0.4 mmol), and triethylamine (0.04 g, 0.8 mmol) in methanol (30 mL) was stirred for 1 h and $DyCl_3{\cdot}6H_2O$ (0.148 g, 0.4 mmol) was added. The solution turned light yellow. It was then stirred for 3 h and filtered. Upon slow evaporation over one week the filtrate yielded X-ray quality light yellow block crystals (45% yield). Elemental analysis (%) calcd for $C_{49}H_{67}Dy_3N_6O_{28}$: C 35.12, H 4.03, N 5.02; found: C 34.64, H 4.03, N 5.04; IR (KBr disc): $\tilde{\nu}$=3194 (w), 1630 (w), 1601 (m), 1463 (s), 1384 (w), 1332 (w), 1274 (m), 1241 (m), 1219 (s), 1077 (m), 957 (m), 853 (w), 783 (w), 739 cm$^{-1}$ (m).

**Synthesis of [Dy$_3$(MeOsalox)$_2$(MeosaloxH)$_4$(NO$_3$)(MeOH)]·MeOH·0.5H$_2$O (2)**: Complex **3** was synthesized following the same procedure as described for **1** but with $Dy(NO_3)_3{\cdot}5H_2O$ (0.173 g, 0.4 mmol) instead of $DyCl_3{\cdot}6H_2O$. The light yellow crystals (yield: 30%) were obtained by slow evaporation of methanol over five days. Elemental analysis (%) calcd for $C_{50}H_{55}Dy_3N_7O_{23.5}$: C 37.13, H 3.43, N 6.06; found: C 37.06, H 3.58, N 5.96; IR (KBr disc): $\tilde{\nu}$=2942 (w), 2839 (w), 1630 (w), 1600 (w), 1463 (s), 1439 (m), 1384 (s), 1333 (w), 1294 (m), 1274 (m), 1240 (m), 1220 (m), 1096 (m), 1077 (m), 1033 (m), 956 (s), 851 (w), 756 (m), 738 cm$^{-1}$ (m).

**Synthesis of [Dy$_3$(MeOsalox)$_2$(MeOsaloxH)$_4$(MeOH)(Cl$_3$CCO$_2$)]·MeOH (3)**: *o*-Vanillin (0.061 g, 0.4 mmol), hydroxylamine chloride (0.028 g, 0.4 mmol), trichloroacetic acid (0.033 g, 0.2 mmol), and triethylamine (0.122 g, 1.2 mmol) were dissolved in methanol (30 mL) stirring for 1 h. $DyCl_3{\cdot}6H_2O$ (0.148 g, 0.4 mmol) was then added. After stirring for 3 h the solution was filtered and the filtrate was left undisturbed to give light yellow crystals of **3** (yield: 25%) within two weeks. Elemental analysis (%) calcd for $C_{52}H_{54}Cl_3Dy_3N_6O_{22}$: C 36.55, H 3.19, N 4.92; found: C 36.92, H 3.03, N 4.83; IR (KBr disc): $\tilde{\nu}$=2941 (w), 1704 (w), 1601 (w), 1462 (s), 1384 (m), 1273 (m), 1240 (m), 1221 (m), 1076 (m), 1035 (w), 956 (m), 851 (w), 756 cm$^{-1}$ (m).

**Synthesis of [Tb$_3$(MeOsalox)$_2$(MeosaloxH)$_4$(NO$_3$)(MeOH)]·MeOH·1.5H$_2$O (4)**: A mixture of *o*-vanillin (0.061 g, 0.4 mmol), hydroxylamine chloride (0.028 g, 0.4 mmol), and triethylamine (0.04 g, 0.8 mmol) in methanol (30 mL) was stirred for 1 h and $Tb(NO_3)_3{\cdot}5H_2O$ (0.174 g, 0.4 mmol) was added. The solution turned light yellow. It was then stirred for 3 h and filtered. Upon slow evaporation over one week the filtrate yielded X-ray quality light yellow block crystals (45% yield). Light yellow block crystals were afforded (54% yield). Elemental analysis (%) calcd for $C_{50}H_{57}N_7O_{24.5}Tb_3$: C 36.96, H 3.54, N 6.03; found: C 36.81, H 3.65, N 5.98; IR (KBr disc): $\tilde{\nu}$=431 (w), 2941 (w), 2839 (w), 1632 (w), 1601 (w), 1464 (s), 1384 (m), 1337 (w), 1294 (m), 1274 (m), 1240 (m), 1220 (s), 1096 (w), 1077 (m), 956 (s), 854 (w), 740 (m).

**Synthesis of [Tb$_3$(MeOsalox)$_2$(MeosaloxH)$_4$Cl(MeOH)][Tb$_3$(MeOsalox)$_2$(MeosaloxH)$_4$Cl(H$_2$O)]·H$_2$O (5)**: This compound was prepared in a similar manner to **4** except using $TbCl_3{\cdot}6H_2O$ instead of $Tb(NO_3)_3{\cdot}5H_2O$. The light yellow needle crystals were obtained by slow evaporation of methanol over ten days (yield: 20%). IR (KBr disc): $\tilde{\nu}$= 2943 (w), 2839 (w), 2158 (s), 1630 (w), 1601 (w), 1464 (s), 1384 (m), 1338 (w), 1293 (w), 1240 (s), 1219 (s), 1077 (m), 987 (s), 853 (w), 740 cm$^{-1}$ (m).

**X-ray crystallography**: Diffraction data for compounds **1** and **4** were recorded on an Oxford Diffraction Gemini R CCD diffractometer with Mo$_{K\alpha}$ radiation ($\lambda$=0.71073 Å) at 150 K. Data collection and processing (cell refinement, data reduction and absorption) were performed using the program PROCESS-AUTO.[19] Diffraction data for compounds **2**, **3** and **5** were recorded on a Rigaku R-AXIS SPIDER Image Plate diffractometer with graphite-monochromated Mo$_{K\alpha}$ radiation ($\lambda$=0.71073 Å). Processing data was accomplished with use of the program SAINT; an absorption correction based on symmetry equivalent reflections was applied using the SADABS program.[20] The structures were solved by direct methods, and all non-hydrogen atoms were refined anisotropically by least-squares methods on $F^2$ using the SHELXTL program.[21] Hydrogen atoms on organic ligands were generated by the riding mode. Crystal data as well as details of data collection and refinements for **1**–**5** are summarized in Table 5.

CCDC-751396 (**1**), CCDC-751397 (**2**), CCDC-751398 (**3**), CCDC-784940 (**4**) and CCDC-784941 (**5**) contain the supplementary crystallographic data for this paper. These data can be obtained free of charge from The Cambridge Crystallographic Data Centre via www.ccdc.cam.ac.uk/data_request/cif.

## Acknowledgements

This work was supported by the NSFC (Grant nos 20525102, 20821001, 90922009 and 50872157) and the "973 Project" (2007CB815305).

---

[1] a) R. Sessoli, D. Gatteschi, A. Caneschi, M. A. Novak, *Nature* **1993**, *365*, 141; b) R. Sessoli, H. L. Tsai, A. R. Schake, S. Wang, J. B. Vin-

cent, K. Folting, D. Gatteschi, G. Christou, D. N. Hendrickson, *J. Am. Chem. Soc.* **1993**, *115*, 1804.

[2] D. Gatteschi, R. Sessoli, *Angew. Chem.* **2003**, *115*, 278; *Angew. Chem. Int. Ed.* **2003**, *42*, 268.

[3] a) Z. Zheng, *Chem. Commun.* **2001**, 2521; b) C. Benelli, D. Gatteschi, *Chem. Rev.* **2002**, *102*, 2369; c) R. Sessoli, A. K. Powell, *Coord. Chem. Rev.* **2009**, *253*, 2328.

[4] X.-J. Kong, Y. Wu, L.-S. Long, L.-S. Zheng, Z. Zheng, *J. Am. Chem. Soc.* **2009**, *131*, 6918.

[5] S. C. Xiang, S. M. Hu, T. L. Sheng, R. B. Fu, X. T. Wu, X. D. Zhang, *J. Am. Chem. Soc.* **2007**, *129*, 15144.

[6] a) M.-B. Zhang, J. Zhang, S.-T. Zheng, G.-Y. Yang, *Angew. Chem.* **2005**, *117*, 1409; *Angew. Chem. Int. Ed.* **2005**, *44*, 1385; b) C.-J. Li, Z.-J. Lin, M.-X. Peng, J.-D. Leng, M.-M. Yang, M.-L. Tong, *Chem. Commun.* **2008**, 6348; c) T. Xu, L.-Z. Li, H.-W. Ji, *Hecheng Huaxue* **2004**, *12*, 22.

[7] a) N. Ishikawa, M. Sugita, T. Ishikawa, S. Koshihara, Y. Kaizu, *J. Am. Chem. Soc.* **2003**, *125*, 8694; b) N. Ishikawa, M. Sugita, W. Wernsdorfer, *J. Am. Chem. Soc.* **2005**, *127*, 3650; c) K. Bernot, J. Luzon, L. Bogani, M. Etienne, C. Sangregorio, M. Shanmugam, A. Caneschi, R. Sessoli, D. Gatteschi, *J. Am. Chem. Soc.* **2009**, *131*, 5573; d) M. A. AlDamen, J. M. Clemente-Juan, E. Coronado, C. Martí-Gastaldo, A. Gaita-Ariño, *J. Am. Chem. Soc.* **2008**, *130*, 8874; e) F. Branzoli, P. Carretta, M. Filibian, G. Zoppellaro, M. J. Graf, J. R. Galan-Mascaros, O. Fuhr, S. Brink, M. Ruben, *J. Am. Chem. Soc.* **2009**, *131*, 4387.

[8] a) J. Tang, I. J. Hewitt, N. T. Madhu, G. Chastanet, W. Wernsdorfer, C. E. Anson, C. Benelli, R. Sessoli, A. K. Powell, *Angew. Chem.* **2006**, *118*, 1761; *Angew. Chem. Int. Ed.* **2006**, *45*, 1729; b) L. F. Chibotaru, L. Ungur, A. Soncini, *Angew. Chem.* **2008**, *120*, 4194; *Angew. Chem. Int. Ed.* **2008**, *47*, 4126; c) J. Luzon, K. Bernot, I. J. Hewitt, C. E. Anson, A. K. Powell, R. Sessoli, *Phys. Rev. Lett.* **2008**, *100*, 247205; d) B. Hussain, D. Savard, T. J. Burchell, W. Wernsdorfer, M. Murugesu, *Chem. Commun.* **2009**, 1100; e) L. Ungur, W. Van den Heuvel, L. F. Chibotaru, *New J. Chem.* **2009**, *33*, 1224.

[9] A. M. Ako, I. J. Hwewitt, V. Mereacre, R. Clérac, W. Wernsdorfer, C. E. Anson, A. K. Powell, *Angew. Chem.* **2006**, *118*, 5048; *Angew. Chem. Int. Ed.* **2006**, *45*, 4926.

[10] a) P.-H. Lin, T. J. Burchell, R. Clérac, M. Murugesu, *Angew. Chem.* **2008**, *120*, 8980; *Angew. Chem. Int. Ed.* **2008**, *47*, 8848; b) I. J. Hewitt, Y. Lan, C. E. Anson, J. Luzon, R. Sessoli, A. K. Powell, *Chem. Commun.* **2009**, 6765.

[11] a) J.-P. Costes, J. M. Clemente-Juan, F. Dahan, F. Nicodème, M. Verelst, *Angew. Chem.* **2002**, *114*, 333; *Angew. Chem. Int. Ed.* **2002**, *41*, 323; b) S. T. Hatscher, W. Urland, *Angew. Chem.* **2003**, *115*, 2969; *Angew. Chem. Int. Ed.* **2003**, *42*, 2862; c) M. Hernandez-Molina, C. Ruiz-Perez, T. Lopez, F. Lloret, M. Julve, *Inorg. Chem.* **2003**, *42*, 5456; d) J.-P. Costes, J.-M. Clemente Juan, F. Dahan, F. Nicodeme, *Dalton Trans.* **2003**, 1272; e) L. E. Roy, T. Hughbanks, *J. Am. Chem. Soc.* **2006**, *128*, 568.

[12] A. Sadoc, R. Broer, C. de Graaf, *J. Chem. Phys.* **2007**, *126*, 134709.

[13] a) K. S. Cole, R. H. Cole, *J. Chem. Phys.* **1941**, *9*, 341; b) Y.-N. Guo, G.-F. Xu, P. Gamez, L. Zhao, S.-Y. Lin, R. Deng, J. Tang, H.-J. Zhang, *J. Am. Chem. Soc.* **2010**, *132*, 8538; c) M. Grahl, J. Kötzler, I. Sessler, *J. Magn. Magn. Mater.* **1990**, *90–91*, 187; d) E. Coronado, C. J. Gómez-García, A. Nuez, F. M. Romero, J. C. Waerenborgh, *Chem. Mater.* **2006**, *18*, 2670.

[14] L. Seijo, Z. Barandiarán in *Computational Chemistry: Reviews of Current Trends, Vol. 4*, (Ed.: J. Leszczynski), World Scientific, Singapur, **1999**, pp. 55–152.

[15] G. Karlström, R. Lindh, P.-Å. Malmqvist, B. O. Roos, U. Ryde, V. Veryazov, P.-O. Widmark, M. Cossi, B. Schimmelpfennig, P. Neogrady, L. Seijo, *Comput. Mater. Sci.* **2003**, *28*, 222.

[16] B. A. Heß, C. M. Marian, U. Wahlgren, O. Gropen, *Chem. Phys. Lett.* **1996**, *251*, 365.

[17] a) L. F. Chibotaru, L. Ungur, C. Aronica, H. Elmoll, G. Pilet, D. Luneau, *J. Am. Chem. Soc.* **2008**, *130*, 12445; b) Programs SINGLE ANISO and POLY ANISO, L. F. Chibotaru, L. Ungur, University of Leuven (Belgium) **2006**.

[18] a) W. Van den Heuvel, L. F. Chibotaru, unpublished; b) A. Soncini, L. F. Chibotaru, *Phys. Rev. B* **2008**, *77*, 220406; c) D. Visinescu, A. M. Madalan, M. Andruh, C. Duhayon, J.-P. Sutter, L. Ungur, W. Van den Heuvel, L. F. Chibotaru, *Chem. Eur. J.* **2009**, *15*, 11808.

[19] PROCESS-AUTO, Rigaku Corporation, Tokyo (Japan), **1998**.

[20] G. M. Sheldrick, SADABS 2.05, University of Göttingen, Göttingen (Germany), **2002**.

[21] SHELXTL 6.10, Bruker Analytical Instrumentation, Madison, Wisconsin (USA), **2000**.

Received: August 11, 2010